Journal of Catalysis 274 (2010) 99–110

Contents lists available at ScienceDirect

Journal of Catalysis

journal homepage: www.elsevier.com/locate/jcat

Modulation of catalyst particle structure upon support hydroxylation: *Ab initio* insights into Pd_{13} and Pt_{13}/γ-Al_2O_3

Chao Hao Hu [a,1], Céline Chizallet [a], Christophe Mager-Maury [a,b], Manuel Corral-Valero [c], Philippe Sautet [b], Hervé Toulhoat [d], Pascal Raybaud [a,*]

[a] Direction Catalyse et Séparation, IFP-Lyon, Rond-point de l'échangeur de Solaize, BP3, 69360 Solaize, France
[b] Université de Lyon, Institut de Chimie de Lyon, Laboratoire de Chimie, Ecole Normale Supérieure de Lyon and CNRS, 46 allée d'Italie, 69364 Lyon Cedex 07, France
[c] Direction Physique et Analyse, IFP-Lyon, Rond-point de l'échangeur de Solaize, BP3, 69360 Solaize, France
[d] Direction scientifique, IFP, 1 et 4 Avenue de Bois-Préau, 92852 Rueil-Malmaison Cedex, France

ARTICLE INFO

Article history:
Received 26 January 2010
Revised 23 April 2010
Accepted 16 June 2010
Available online 23 July 2010

This paper is dedicated to our deeply missed colleague John Patrick Lynch, PhD from the Cavendish Laboratory, Oxford, Expert Director in Material Sciences and Catalysis at IFP.

Keywords:
Palladium
Platinum
Alumina
Supported catalysts
Density functional theory
Hydroxyls

ABSTRACT

An atomic picture of highly dispersed palladium and platinum catalysts supported on gamma-alumina is provided. Understanding the structure–reactivity relationship in the field of catalysis by metals requires the rationalization of the role of the metal-support interaction on the morphology and electronic properties of nanometer size metallic particles. Thus, the interaction energies and the structures of Pd_{13} and Pt_{13} clusters deposited on two relevant gamma-alumina surfaces are systematically investigated by density functional theory calculations. The hydroxylation of the support weakens the metal adhesion and influences the cluster morphologies. Flat lying bi-planar clusters with strong interaction energies are stabilized on the dehydrated (1 0 0) surface, whereas clusters with a three-dimensional morphology are favored by the hydroxyl groups of the (1 1 0) surface. A consistent comparison of Pt and Pd is achieved. The shortest metal–oxygen (M–O) bond distances calculated by DFT agree well with EXAFS M–O distances. Moreover, the presence of metal–aluminum bond distances close to 2.61–2.64 Å may explain experimental features. The present work also provides structural and electronic clues for the understanding of the reactivity of highly dispersed Pd and Pt catalysts.

1. Introduction

In recent years, nanoscale transition metal clusters supported on metal oxide substrates have attracted much attention due to their important industrial applications in heterogeneous catalysis [1–3], fuel cell technologies, magnetism, optics or microelectronics among others [4,5]. The chemical reactivity and selectivity for many systems are known to be intimately related to the size and shape of the metal particles and to the choice of the oxide support [6–10]. Understanding the metal-support interaction (MSI) is thus the first step toward the design of tailor-made catalysts with desired properties [5,11]. However, despite continuous improvements of physical characterization tools [8,12–19], it remains hard to provide complete information on the structure of metal–oxide interfaces that depends strongly on the size of the metallic cluster, particularly when smaller than 1 nm. One important reason is related to the dynamic structural flexibility of metallic clusters with such sizes and when supported on oxide surfaces [20]. Moreover, the subnanometric structure of these highly dispersed systems is suspected to be strongly sensitive to the environment to which they are exposed, either in a characterization chamber or in reaction conditions.

Pd or Pt clusters supported on alumina have been widely used for several catalytic applications such as petroleum refining, petrochemistry and automotive exhaust treatment. In particular, γ-alumina is considered as one of the most versatile oxide supports due to its high degree of porosity and surface area (200–240 m^2/g) [21]. Moreover, its different surfaces exhibit specific acid–base properties, leading to tunable improvement in the catalyst activity. In fundamental studies, many experiments have been devoted to the growth and structure of Pd and Pt clusters natively reduced on alumina films [11,13,18,19,22–30], considered as model catalysts. Using transition electron microscopy (TEM) and scanning tunneling microscopy (STM), it is generally concluded that for

* Corresponding author. Fax: +33 478022066.
E-mail addresses: chaohao.hu@guet.edu.cn (C.H. Hu), celine.chizallet@ifp.fr (C. Chizallet), christophe.mager-maury@ifp.fr (C. Mager-Maury), manuel.corral-valero@ifp.fr (M. Corral-Valero), philippe.sautet@ens-lyon.fr (P. Sautet), herve.toulhoat@ifp.fr (H. Toulhoat), pascal.raybaud@ifp.fr (P. Raybaud).
[1] Present address: School of Materials Science and Engineering, Guilin University of Electronic Technology, Guangxi 541004, People's Republic of China.

0021-9517/$ - see front matter © 2010 Elsevier Inc. All rights reserved.
doi:10.1016/j.jcat.2010.06.009

effective Pd or Pt coverage lower than one monolayer, the size of the metallic particles falls within the 1–2 nm range and that the shape of the particles is rather flat, which suggests a good wetting and spreading of the metal over the support. A contraction of the lattice parameter is also noticed from electron diffraction techniques for the smallest clusters, when compared to the bulk metal [24]. Pt clusters seem to grow almost epitaxially on an ultrathin film model of alumina support, formed by controlled oxidation of a NiAl substrate [24,29], but the structure of this surface oxide is complex and different from that of γ-alumina [31,32]. Under these conditions, Pd clusters mainly exhibit (1 1 1) facets even for the smallest sizes [30]. Such model alumina surfaces are usually pristine and not covered with hydroxyl groups, thanks to very accurate control of the residual water pressure. However, in the case of model Rh/Al_2O_3 samples, the group of Freund [33] has, shown that the hydroxylation state of the alumina films is determinant for the size and distribution of the particles on the support. The question of the influence of the hydroxylation state of the alumina surface thus stands as one of the major points to be addressed, similarly to the question of the crucial influence of point defects on some other oxides like TiO_2 and MgO [17,34–36].

Real catalysts are indeed usually synthesized by impregnation of palladium or platinum salts in aqueous solution on the alumina powder support, followed by calcination and reduction steps [2,37]. Here again, the influence of hydroxyl groups is critical throughout the synthesis sequence. To allow accessibility of a maximum number of metal sites, the highest Pt or Pd dispersion, e.g. the smallest metallic particles, is aimed at. TEM (with resolution limits) and X-ray absorption spectroscopy such as EXAFS or XANES (following the precursory works of Sinfelt and coworkers [38,39]) have been extensively used for the characterization of such highly dispersed catalysts [40–50]. A relevant industrial example is highlighted by the bifunctional reforming catalysts such as γ-alumina-supported bimetallic PtX bimetallic (X = Re, Ir, or Sn), where particles size are usually below 1 nm.

Such small particle sizes (below 1 nm) are commonly obtained for platinum, with an estimated average number of metal atoms in the range between 11 and 14, and with nearest neighbor metal–metal coordination numbers around 4–7 (versus 12 in bulk Pd or Pt), the exact value depending strongly on synthesis conditions (mainly reduction [41] linked to hydrogen desorption [42]). In some cases, Pt–O bonds have been detected [40–42], whereas Pt–Al bonds are usually not invoked. Highly dispersed palladium particles, with similar sizes (∼1 nm) and coordination numbers, are more scarcely reported and characterized [48,51].

Beyond these important experimental insights, a more accurate atomic description of the interface between the Pd or Pt particles and Al_2O_3 surface remains a challenging question, which *ab initio* molecular modeling may efficiently address. Several first-principles studies of the alumina-supported Pd or Pt systems based on density functional theory (DFT) have been reported in the literature. They differ first in the nature of the alumina surface model. Most often, ideal surfaces of α-Al_2O_3 have been considered [52–66], so that a clear interest remains in modeling the metal/γ-Al_2O_3 interface, γ-alumina being the most frequently used support in industry (such as in catalytic reforming process). γ-Alumina has indeed a bulk and surface structure different from that of α-alumina, in particular with 25% of the Al atoms in tetrahedral coordination [67]. The hydroxylation state of the support is addressed in some studies [65,66,68–70]; however, its influence on the morphology of a cluster of significant size (more than 10 atoms) is very scarcely analyzed. Indeed, the size of the metal clusters in interaction with the support is for the most part reduced to a single atom [55,56,58,59,61,62,64–66,70,71] or sometimes extends up to five atoms [54,57,60,63,69,72]. Such systems reflect basic chemical trends and the initial process of nucleation of metal particles on oxide surfaces; however, the up to now simulated sizes remain well below the real sizes of high dispersion oxide-supported metal clusters with diameters distributed around 1 nm. Only a few works deal with more significant cluster sizes supported on fully dehydrated alumina (Pt_{10} in Ref. [73] and Pt_{19} in Ref. [74]), but the morphology of the cluster is either arbitrarily chosen for a further study of its reactivity [74] or not discussed [73]. For relevant applications in catalysis, the challenging question of the shape of nanometer size Pt and Pd particles supported on γ-Al_2O_3 as a function of the hydroxylation state of the support remains to be addressed in a quantitative manner.

In the same spirit as for our previous DFT studies on the nucleation of small Pd_n ($n = 1–5$) clusters on γ-Al_2O_3 surfaces [68,69,75], taking advantage of our previous exploration of the gas phase morphology of 13-atom late transition metal clusters, on the one hand [76], and of the surface model for γ-Al_2O_3 established in our group on the other hand [77–79], we expand our study in the present work to the investigation of the interaction between Pd_{13} and Pt_{13} clusters with various shapes and dehydrated (1 0 0) and hydroxylated (1 1 0) γ-Al_2O_3 surfaces. Our aim is to elucidate the nature of the metal-support interaction, in connection with the absence or presence of hydroxyl groups on these two γ-alumina surfaces, serving as reference models for realistic catalytic conditions. We also determine structural and electrostatic properties likely to orient the reactivity of the clusters during catalysis.

2. Methods

The dehydrated (1 0 0) and hydroxylated (1 1 0) surfaces of γ-Al_2O_3 (8.9 OH nm^{-2}, in agreement with thermodynamic analysis and with experimental measurements [80]) from Refs. [77,78] were modeled with (2×2) supercells and four layer thick slabs as presented in Fig. 1a and b, which contain 160 and 200 atoms, respectively (lattice parameter $a = 11.14$ Å, $b = 16.79$ Å and $a = 16.14$ Å, $b = 16.79$ Å for (1 0 0) and (1 1 0) respectively).

The large area allows M_{13} (M = Pd or Pt) clusters to be accommodated with minimal lateral interactions between periodic images in most cases. In one exceptional case (mentioned in Table 1), the cell has been enlarged (by a factor of 2 in direction *a*) to avoid excessive lateral interactions. Considering the local Al, O, and OH environments present on the two surfaces and guided by our previous systematic explorations of the potential energy surface for Pd and Pd_4 clusters [68,69], three relevant adsorption sites for each surface were chosen and named as A–C sites as marked in Fig. 1a and b, above which the center of mass of the M_{13} cluster was initially placed. Based on our previous work on the morphology trends of 4*d* and 5*d* late transition metal 13-atom clusters [76], a reliable structure database for isolated Pd_{13} and Pt_{13} clusters was used to explore possible structural configurations on γ-Al_2O_3 surfaces. As shown in Fig. 1c, we considered some common structures including cuboctahedron (CUB), buckled biplanar (BBP), new biplanar (NBP), and top-capped simple cubic (TCSC). The most stable isomer for Pd_{13} from first-principles molecular dynamics simulations based on the simulated annealing (SA) method at 800 K (hereafter Pd_SA) and the two stable isomers for Pt_{13} from the SA simulations at 1000 and 2000 K (hereafter Pt_SA1 and Pt_SA2, respectively) were also considered. To scan a sufficiently large configuration space, four initial structural configurations on each adsorption site were further considered by rotating and inverting each metal cluster, and named as A1, A2, A3, A4, B1, etc. In the following, Ai for example will depict configurations in which the M_{13} cluster is located in the A region, the i label depicting the order of decreasing stability (from the highest to the lowest, as deduced from binding energies, see further).

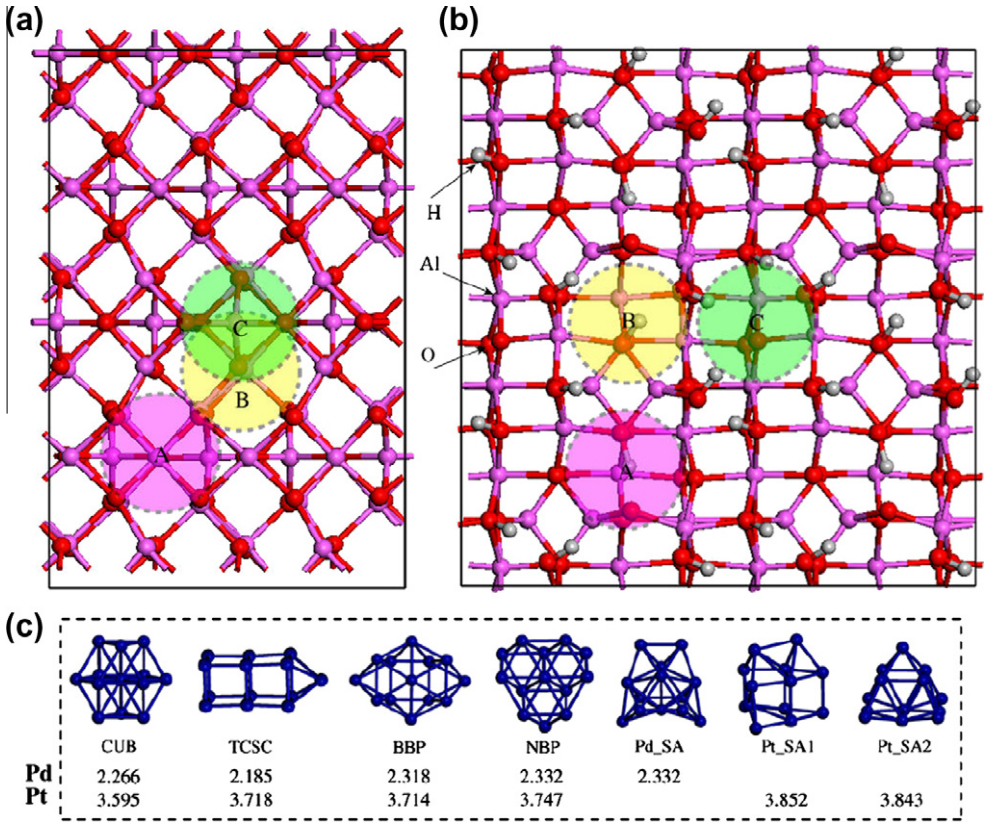

Fig. 1. (a) Dehydrated (1 0 0) and (b) hydroxylated (1 1 0) surfaces of γ-Al_2O_3: Al, O, and H atoms are shown as purple, red, and gray balls, respectively. Three adsorption sites for the (1 0 0) and (1 1 0) surfaces are marked by circles with shaded-purple, shaded-yellow, and shaded-green colors (named A, B, and C sites, respectively). (c) The low-energy Pd_{13} and Pt_{13} clusters considered with the most relevant structures (see text for explanation). The calculated binding energies (eV/atom) of isolated clusters are reported in the first and second rows. (For interpretation of the references to color in this figure legend, the reader is referred to the web version of this article.)

Table 1
Binding energies E_b, Bader electrostatic charge of M_{13} clusters, mean coordination number N, average optimized inter-atomic distances d, for selected Pd_{13} and Pt_{13} clusters supported on γ-Al_2O_3 (1 0 0) and (1 1 0) surfaces. The calculated values for the corresponding isolated M_{13} clusters are listed in parenthesis. Systems are ranked by order of stability, as given by E_b (see text for definition).

Model		E_b (eV/atom)	Bader charge of M_{13} (e)	M–O		M–Al [M–H if reverse spillover]		M–M	
				N	d (Å)	N	d (Å)	N	d (Å)
Pd_{13}/γ-Al_2O_3									
On (100)	NBP (A1)	2.53 (2.33)	−0.34	0.5	2.384	0.1	2.618	5.5	2.713 (2.695)
	BBP (B1)	2.52 (2.32)	−0.07	0.3	2.208	0.3	2.828	5.4	2.709 (2.693)
	TCSC (C1)[b]	2.47 (2.19)	−0.35	0.3	2.226	0.2	2.514	4.9	2.707 (2.578)
	Pd_SA (C1)	2.46 (2.33)	−0.26	0.2	2.159	0.2	2.792	5.1	2.708 (2.713)
	CUB (B1)[b]	2.45 (2.27)	−0.35	0.4	2.214	0.1	2.369	5.4	2.712 (2.700)
On (110)	Pd_SA (A1)	2.45 (2.33)	0.09	0.2	2.187	0	–	5.7	2.717 (2.713)
	NBP (A1)	2.44 (2.33)	0.09	0.2	2.238	0	–	5.5	2.701 (2.695)
	BBP (A1)	2.43 (2.32)	0.18	0.3	2.440	0	–	4.8	2.704 (2.693)
	Pd_SA after H migration	2.49 (2.33)	0.53	0.3	2.217	0 [0.2]	–[1.820]	5.5	2.717 (2.713)
Pt_{13}/γ-Al_2O_3									
On (100)	NBP (C1)	4.04 (3.75)	−0.99	0.5	2.192	0.4	2.643	4.8	2.691 (2.651)
	Pt_SA2 (C1)	4.02 (3.84)	−0.12	0.4	2.266	0.2	2.831	4.6	2.642 (2.656)
	TCSC (C1)	4.02 (3.72)	−0.29	0.5	2.155	0.3	2.810	3.5	2.602 (2.557)
	BBP (B1)[a]	3.99 (3.73)	−0.27	0.3	2.155	0.2	2.599	4.5	2.651 (2.647)
	Pt_SA1 (B1)	3.99 (3.85)	−0.13	0.3	2.288	0	–	4.3	2.635 (2.623)
	CUB (B1)[b]	3.92 (3.60)	−0.12	0.2	2.236	0.1	2.514	4.9	2.669 (2.668)
On (110)	Pt_SA2 (C1)	3.97 (3.84)	−0.01	0.2	2.183	0	–	4.9	2.657 (2.656)
	Pt_SA1 (A1)	3.96 (3.85)	−0.16	0.2	2.228	0	–	4.3	2.609 (2.623)
	NBP (B1)	3.92 (3.75)	−0.11	0.2	2.145	0	–	4.9	2.665 (2.651)
	Pt_SA2 after 1H migration	4.00 (3.84)	0.30	0.3	2.124	0 [0.1]	–[1.555]	4.9	2.660 (2.656)
	Pt_SA2 after 2H migration	4.02 (3.84)	0.70	0.3	2.077	0 [0.2]	–[1.560]	4.9	2.663 (2.656)

[a] This simulation has been undertaken in a double supercell.
[b] These clusters are unstable once adsorbed on the alumina surface and strongly reconstruct upon adsorption (the energy value includes this strong reconstruction).

The periodic DFT geometry optimizations were performed using a plane-wave method as implemented in the Vienna *Ab initio* Simulation Package (VASP) [81,82]. The exchange–correlation functional was treated within the generalized gradient approximation (GGA) parameterized by Perdew and Wang PW91 [83], and the electron–ion interaction was described by the projector augmented wave (PAW) scheme [84,85]. Spin-polarized calculations used the interpolation formula of Vosko, Wilk, and Nusair [86]. We verified that the use of an energy cutoff of 400 eV ensured a good convergence of the total energies. Gaussian smearing with $\sigma = 0.02$ eV has been used. Since our alumina surface unit cells are large, the Brillouin zone was only sampled at the Γ point for the (1 1 0)-based surface models, and with a $2 \times 1 \times 1$ grid for the (1 0 0)-based models. The bottommost two layers were fixed to the positions of the relaxed alumina slabs, while the other top atomic layers of (1 0 0) and (1 1 0) slabs, together with the adsorbed M_{13} clusters, were fully relaxed until the total energy change between two successive ionic optimization steps was less than 10^{-4} eV. Dipolar corrections were applied to account for the arbitrary electrostatic interaction between the asymmetric – thus polar – slab sides. The electron localization function (ELF [87,88]), electronic density differences (inherent to the adsorption step) and Bader charges[89,90] were calculated at the same level of theory, with an increased precision of the energy cutoff up to 520 eV.

Generally, the binding energy of isolated 13-atoms gas phases M_{13} $\left(E_b^{M_{13}}\right)$ can be defined by the following equation:

$$E_b^{M_{13}} = \{13 \times E(M) - E(M_{13})\}/13 \quad (1)$$

where $E(M_{13})$ and $E(M)$ are the total energies of M_{13} clusters and of a free M atom, respectively. Similarly, the binding energy of M_{13} supported on γ-Al_2O_3 surfaces $\left(E_b^{M_{13}/Al_2O_3}\right)$ per metallic atom is given by the following equation:

$$E_b^{M_{13}/Al_2O_3} = \{13 \times E(M) + E(Al_2O_3) - E(M_{13}/Al_2O_3)\}/13 \quad (2)$$

where $E(M_{13}/Al_2O_3)$ and $E(Al_2O_3)$ are the total energies of supported systems and of alumina slabs without M_{13} clusters, respectively. $E_b^{M_{13}/Al_2O_3}$ reflects the stability of the adsorbed M_{13} clusters on the γ-Al_2O_3 surfaces and not the cohesion of the supported metallic cluster alone. In addition, it should be noted that from Eqs. (1) and (2), the adsorption energy of M_{13} on alumina $\left(E_{ads}^{M_{13}/Al_2O_3}\right)$ can be further deduced from the energy difference between $E_b^{M_{13}/Al_2O_3}$ and $E_b^{M_{13}}$ and given by the following equation:

$$\begin{aligned} E_{ads}^{M_{13}/Al_2O_3} &= 13 \times \left(E_b^{M_{13}} - E_b^{M_{13}/Al_2O_3}\right) \\ &= E(M_{13}/Al_2O_3) - E(Al_2O_3) - E(M_{13}) \end{aligned} \quad (3)$$

Moreover, interaction energies are defined by the following equation:

$$E_{int}^{M_{13}/Al_2O_3} = E(M_{13}/Al_2O_3) - E(Al_2O_3') - E(M_{13}') \quad (4)$$

where $E(Al_2O_3')$ is the energy of the surface fragment with the deformed geometry after adsorption of the M_{13} cluster, and $E(M_{13}')$ the energy of the M_{13} cluster with the deformed geometry after its adsorption on the alumina surface. Deformation energies, defined by Eqs. (5) and (6) for the alumina support and the metallic cluster, respectively, enable the impact of the shape adaptation on the adsorption process to be quantified. The total deformation energy is given by Eqs. (7) and (8) which makes the link between the adsorption, interaction, and deformation energies.

$$E_{def}^{Al_2O_3} = E(Al_2O_3') - E(Al_2O_3) \quad (5)$$

$$E_{def}^{M_{13}} = E(M_{13}') - E(M_{13}) \quad (6)$$

$$E_{def}^{tot} = E_{def}^{M_{13}} + E_{def}^{Al_2O_3} \quad (7)$$

$$E_{ads}^{M_{13}/Al_2O_3} = E_{int}^{M_{13}/Al_2O_3} + E_{def}^{tot} \quad (8)$$

Note that binding energies are usually defined as positive for stable systems when compared to isolated atoms, whereas adsorption, interaction, and deformation energies are defined negatively for exothermic reactions, as usually chosen in thermodynamics. To distinguish the adsorption energetics of M_{13} on different surfaces and also to facilitate the following discussion, the notations $E_b^{M_{13}/Al_2O_3}$, $E_{ads}^{M_{13}/Al_2O_3}$ and $E_{int}^{M_{13}/Al_2O_3}$ are further simplified into $E_b^{M_{13}/(100)}$, $E_{ads}^{M_{13}/(100)}$ and $E_{int}^{M_{13}/(100)}$ for dehydrated (1 0 0) surface, and $E_b^{M_{13}/(110)}$, $E_{ads}^{M_{13}/(110)}$ and $E_{int}^{M_{13}/(110)}$ for hydroxylated (1 1 0) surface.

Additionally, bond overlap population (BOP [91]) and Mulliken charge analyses have been performed on the same periodic systems with the CASTEP code [92], using the same general parameters as for the VASP calculations, except for the use of ultrasoft pseudopotentials [93] with an energy cutoff of 340 eV. Population analysis in CASTEP consists in the projection of the plane-wave states onto a localized basis, using a technique described by Sanchez-Portal et al. [94], followed by analysis of the resulting projected states with the Mulliken formalism [95].

3. Results

3.1. M_{13} interacting with the dehydrated γ-Al_2O_3 (1 0 0) surface

3.1.1. Energetic analysis

The calculated binding energies $E_b^{M_{13}/(100)}$ and $E_b^{M_{13}/(110)}$ for Pd_{13} and Pt_{13} supported on (1 0 0) surfaces are compiled in Supplementary material S1. Table 1 summarizes the energetic, atomic charge, and geometric features of the most stable configurations (A1, B1, or C1) found for each starting geometry of the M_{13} cluster. More extended data on energetic, magnetic, and electronic properties are provided in Supplementary material S2.

The adsorption process usually leads to a stabilization of the system, as shown by the higher binding energies in the supported state than in the gas phase. Several structures remain competitive, in particular in the case of platinum clusters, which relates to the difficulties experimentally encountered for their detailed structural characterization. The order of stability of clusters in the gas phase is not necessarily retained on the dehydrated alumina surface and some inversions are observed, underlining the key role of the support.

Moreover, the alumina site where the cluster is the most stabilized (A, B, or C) depends on the morphology of the cluster, which suggests very specific interactions with several atoms of the cluster, thus requiring a matching between the oxide surface atomic network and the metallic atoms. Note that the alumina support quenches partially or totally the spin polarization upon mixing of metal states with O and Al states (see Supplementary material S2).

The most stable M_{13}/γ-Al_2O_3 (1 0 0) configurations involve the cluster in the NBP geometry, both for palladium and for platinum. The isolated NBP cluster exhibits a high C_{3v} symmetry and consists in two layers: the first one contains six atoms forming a triangular pattern and the second layer contains seven atoms forming a hexagonal pattern. On γ-Al_2O_3 (1 0 0), the NBP clusters preferentially adsorb with the seven atoms layer contacting with alumina, as depicted in Fig. 2a and b (some other optimized stable structural configurations A1, B1, or C1 are displayed in Supplementary material S3).

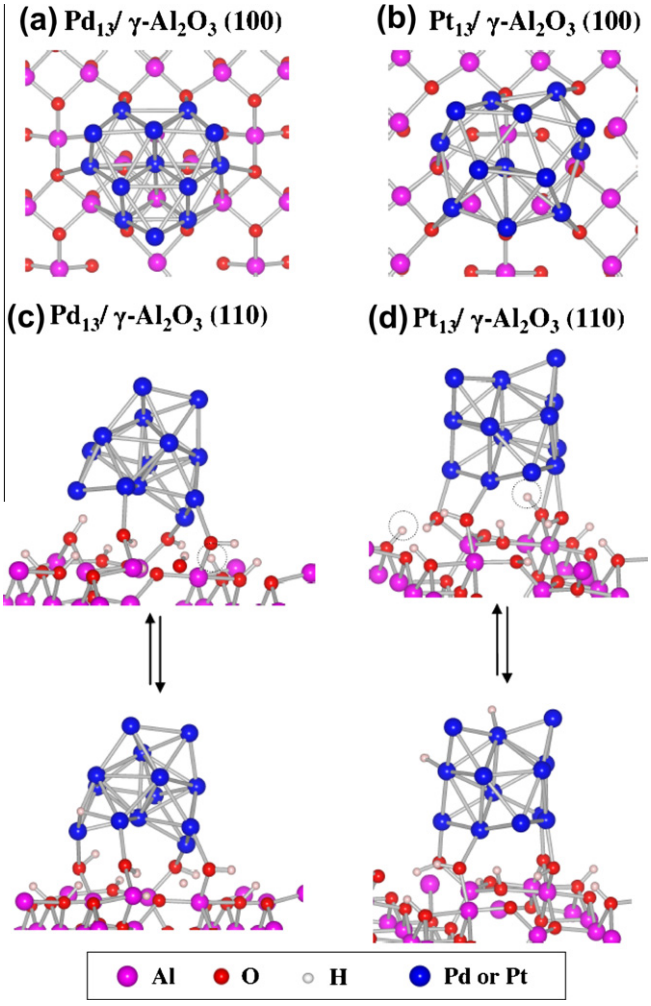

Fig. 2. Ball and stick representations of the atomic structures of: (a) Pd_{13}-NBP in position A1 and (b) Pt_{13}-NBP in position C1 respectively supported on dehydrated γ-Al_2O_3 (1 0 0) (most stable structures, top views). Corresponding side views are given in Fig. 3. (c and d) Pd_{13}–Pd_SA and Pt_{13}–Pt_SA2, respectively, supported on hydrated γ-Al_2O_3 (1 1 0) (most stable structures), before (top) and after (bottom) hydrogen reverse spillover. Hydrogen atoms involved in the reverse spillover process are circled with dotted lines in (c) and (d).

For Pd, the second most stable geometry (energetically very close to NBP) is the BBP morphology which is also a bi-layer type cluster. The other supported clusters are less stable. For instance, although the isolated Pd_SA cluster was found energetically degenerate to the isolated NBP-Pd_{13} (see Fig. 1c and Table 1) [76], the most stable configuration for Pd_SA on the (1 0 0) surface is less stable than the supported Pd_{13}-NBP system (about 67 meV/atom in $E_b^{Pd_{13}/(100)}$). For Pt, it is important to underline that the NBP cluster was not found as the most stable for the isolated Pt_{13} nanoparticles, where Pt_SA1 and Pt_SA2 were the preferred structures in the gas phase [76]. The Pt_SA2 cluster becomes the second most stable cluster on the surface. These results suggest that flat clusters are favored on this kind of alumina surface, to optimize the metal-support interaction, even if 3D clusters are sometimes intrinsically more stable in gas phase. This is clearly seen in the adsorption energy which is ~1.5–2 eV more exothermic for flat NBP or BBP compared to 3D SA clusters on the dehydrated (1 0 0) termination (Supplementary material S2). The preferred shape is hence controlled on this surface by the cluster-oxide adhesion. This behavior is also illustrated by the huge deformation of some 3D clusters such as Pt_{13}-CUB (Supplementary material S3), which tends to flatten, so as to maximize the interaction with the support, and which can even lead to a stabilizing reconstruction process as shown by negative deformation energies (Supplementary material S2).

3.1.2. Local structure and electronic analysis

The structural analysis of the interface, in terms of the numbers of M–O and M–Al bonds, is given in Table 1. In each case, the total number of bonds has been determined according to a minimal BOP value criterion (BOP > 0.05). Due to the delocalized nature of the bond in metallic systems, preventing any interpretation of the BOP, the number of M–M bonds within the cluster has been determined on a simple criterion based on distance (d(M–M) <3.0 Å). In the following, the detailed structural and electronic analysis is provided mainly for the most stable supported structures, e.g. M_{13}-NBP. The mean coordination number, N, of metal atoms with other metal atoms ($N = 2N_{tot}/13$) or with oxygen and aluminum atoms ($N = N_{tot}/13$) is also given in Table 1 to allow a direct comparison with experimental data (mainly from EXAFS).

3.1.2.1. Metal cluster features. If we consider the lattice parameter for bulk Pd (about 2.75 Å) and that of bulk Pt (about 2.76 Å [44]), one first general tendency is a contraction of M–M bond lengths either for the isolated clusters or for those supported on dehydrated alumina. This contraction with respect to the bulk is slightly more pronounced for Pt_{13} than for Pd_{13} (mean Pt–Pt distance of 2.69 Å, versus mean Pd–Pd distance of 2.71 Å). Moreover, upon adsorption, the metallic clusters become distorted, resulting in a slight increase in M–M distances (generally by 0.01–0.04 Å) when compared to their gas phase structures. This phenomenon is significantly stronger for platinum than for palladium, as shown from the qualitative distortion in Fig. 2a versus b, and from the increase in d(M–M) (0.7% and 1.5% for Pd_{13}-NBP and Pt_{13}-NBP, respectively, Table 1). This can be explained by the mismatch between Pt–Pt bond lengths (2.65 Å in the gas phase) and O···O or Al···Al distances on the support (typically 2.80 Å). This mismatch is weaker for Pd–Pd bond lengths (2.70 Å in the gas phase). The higher distortion for Pt is also related to the stronger particle support interaction in Pt_{13}, as illustrated by the larger interaction energy and the resulting stronger deformation energy of the cluster (Supplementary material S2).

Except for the Pd_{13}-TCSC cluster, for which the number of M–M bonds increases from 24 to 32, due to extensive reconstruction of the cluster (triangular facets are generated from a square facet cluster, Fig. S3-1-(b) in Supplementary material), the number of M–M bonds decreases for all other clusters, linked to their expansion and distortion. As a first qualitative explanation, we can invoke the fact that the ligand effect of the support induces a weakening of the cluster cohesion as a result of bond order conservation.

To investigate electronic effects in more details, the charge density difference analysis, shown in Fig. 3 for palladium (Supplementary material S4 for Pt), characterizes the effect of the presence of the support on the electronic distribution within the cluster and vice versa. The reference systems for the charge density are the support, and the cluster is independently calculated in the distorted geometry of the interacting system. The evolution of M–M bonds shows similar qualitative features for Pd_{13} and Pt_{13} supported on the (1 0 0) dehydrated alumina surface. In the case of platinum, the changes in the density are stronger than for palladium (the density isosurface is drawn for a value of 0.005 e $Å^{-3}$ for Pt compared to 0.003 e $Å^{-3}$ for Pd). The intensity of the electronic exchanges between the support and the cluster are thus enhanced for Pt with respect to the Pd cluster, in line with the higher structural distortion of the Pt cluster during adsorption. This is particularly true for the interfacial Pt_{13}/(1 0 0) Al_2O_3 region, where the charge is strongly accumulated.

Hence for Pd_{13}, the charge density located on the six uppermost metallic atoms is affected despite being farther from the support.

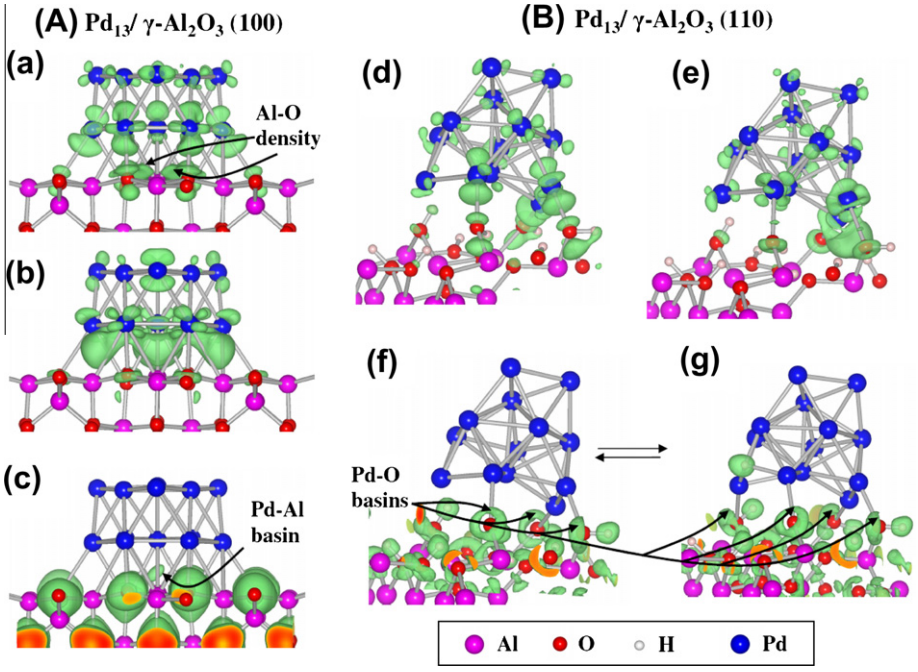

Fig. 3. (A) Charge density difference analysis for Pd_{13}-NBP clusters supported on γ-Al_2O_3 (1 0 0) dehydrated surface, (a) electron depletion and (b) electron accumulation, drawn for absolute isosurface values of 0.003 e Å^{-3}. (c) ELF = 0.7 plot. (B) Charge density difference analysis for the Pd_{13}–Pd_SA cluster deposited on the γ-Al_2O_3 (1 1 0) hydroxylated surface, (d) electron depletion and (e) electron accumulation, drawn for absolute isosurface values of 0.004 e Å^{-3}. (f) ELF = 0.84 plot for the same cluster; (g) ELF = 0.84 plot after hydrogen reverse spillover.

The charge density decrease affects mainly the orbitals localized in the plane parallel to the surface (Fig. 3a). Moreover, the density increases in the direction normal to the surface. This suggests a polarization of the orbitals by the support contributing to the metal support interaction, even for the uppermost layer of metal atoms. As there is almost no overlap between these orbitals (depleted or populated), the distance within the uppermost metal atom layer is only slightly changed when compared to the gas phase (2.66 Å on alumina versus 2.67 Å in the gas phase). For the same reasons, the cohesion between the two layers of palladium atoms is not strongly affected (as can also be seen from the distances between the layers, 2.72 Å on alumina versus 2.71 Å in the gas phase). Finally, for Pt as well as Pd, the density is the most strongly reorganized under the influence of the oxide around the metal atoms in contact with the support. A significant depletion of the density involves orbitals overlapping along the M–M bonds. This is reflected by the partial loss of the cohesion within the lowermost plane of the cluster (2.74 Å on alumina versus 2.69 Å in the gas phase for Pd). Electrons withdrawn from localized orbitals (Fig. 3a) are transferred to much more diffuse states (Fig. 3b) at the metal/support interface. This aspect will be further detailed in the next section.

The electrostatic charge analysis is reported in Table 1 (Bader analysis, which in terms of trends compares rather well with the Mulliken analysis reported in Table S2-1 in the Supplementary material). M_{13} clusters supported on the (1 0 0) dehydrated surface are slightly anionic, in particular for platinum, as a consequence of the charge transfer from the support (isolated clusters are neutral). Detailed analysis of the Bader charge distribution within the clusters (Supplementary material S5) shows that this anionic character mainly corresponds to the Pd and Pt atoms bonded to aluminum atoms.

3.1.2.2. Metal-support interface features. The interaction of the cluster with the dehydrated alumina surface leads to new features at the metal-support interface. Fig. 3a and b and Supplementary material S4 show that d orbitals from the lowermost layer metal atoms, p orbitals from the surface oxygen atoms, and electrons involved in the Al–O bonds before adsorption are contributing to new regions of density accumulation:

- M–O bonds, which can be seen for a lower isosurface value for palladium (not reported). The ELF analysis also demonstrates a slight polarization of the electronic basin along M–O bonds.
- Diffuse density along M–Al bonds, clearly seen from the ELF analysis reported in Fig. 3c, with unambiguous M–Al electronic basins, indicative of a covalent bond. Such chemical bonds have also been shown for Pd and Pt single atoms on various alumina phases [53,58,64,66,68,71], and also for a Pd_4 cluster on the gamma-alumina (1 0 0) surface [75]. As in our previous work [68,75], this charge redistribution is also accompanied by an increase in the electron density in the Al–O bonds near the metal cluster.

Electrostatic charge analysis for atoms of the support, reported in Supplementary material S7, provides a complementary view of this phenomenon. This analysis confirms that oxygen atoms bonded to Pd or Pt atoms are electronically depleted. Their charge is transferred in part to aluminum atoms newly bonded to metal atoms: the M_{13} cluster initiates charge transfer from oxygen atoms to aluminum atoms.

Adsorption of all kinds of clusters but in particular NBP induces a stronger stabilization for platinum (E_{ads} = −3.79 eV, see Table 1) than palladium (−2.58 eV). Indeed, the Pt 5d orbitals are more diffuse than the Pd 4d ones. As a result, the overlap with the support orbitals is larger. This results in a stronger metal–oxide interaction and a more important covalent character at the interface where the charge accumulation is predominant. This is especially visible in the very strong difference in interaction energy but slightly mitigated by the larger induced deformation energy cost for the surface and cluster partners. A slightly higher number of M–O bonds are shown for Pt and, in a counter intuitive manner, the average

Pt–O distance for the NBP adsorption is shorter than the Pd–O one. This leads to a much higher M–O total BOP value (1.30 versus 0.66, see Supplementary material S2), but also to more numerous M–Al bonds and higher associated BOP (0.93 versus 0.18). This result is fully in line with the charge density and ELF analyses.

Note that Pd–Al and Pd–O distances are generally longer for Pd_{13}/γ-Al_2O_3 (1 0 0) than for smaller clusters Pd_n (n = 1–5) on the same (1 0 0) dehydrated alumina surface [69]. However, since these Pd–Al and Pd–O bonds are more numerous, Pd_{13} cluster exhibits stronger adsorption energies. The flatness of the NBP cluster appears as a key feature of a strong adsorption on the dehydrated (1 0 0) alumina surface.

3.2. M_{13} interacting with the hydrated γ-Al_2O_3 (1 1 0) surface

3.2.1. Energetic analysis

The stability of the deposited M_{13} clusters of various geometries on different sites of the hydroxylated (1 1 0) alumina surface is summarized in Table 1 (as for dehydrated alumina, the reader is referred to Supplementary material S1–S3 for more details). When compared to the dehydrated (1 0 0) surface, for similar cluster morphologies, the energy stabilization afforded by adsorption is significantly weaker for the hydroxylated surface (by about 1 eV), as previously found for single atoms and smaller clusters [66,68–70]. This trend is attributed to weaker metal-support interaction energies. The variation in energy for the different configurations studied is narrower than on the non-hydroxylated (1 0 0) surface, which shows that the potential energy surface of the clusters on the hydroxylated (1 1 0) surface is flatter and only slightly depends on the cluster morphology. For Pd_{13} and Pt_{13}, the binding energies of the three most stable clusters (Pd_SA, Pt_SA1, Pt_SA2, NBP, or BBP) are closer to their value in the gas phase, indicating that the support effect induced by the hydrated surface is significantly weakened. In particular, Pd_SA and Pt_SA2 morphologies which are of spherical type become stable versus the flat bi-layer type.

3.2.2. Local structure and electronic analysis

The M–M bond lengths (Table 1) and the number of M–M bonds are only slightly perturbed after adsorption, in line with the adsorption and interaction energies lower than for the dehydrated surface. No localized M–Al bond is visible, and the adsorption process mainly occurs through the formation of M–O(H) bonds. Monocoordinated μ_1–OH are the only OH groups involved in the metal-support interaction, due to their orientation protruding outwards from the surface.

The most stable supported structures correspond to Pd_SA and Pt_SA2, as depicted in the upper parts of Fig. 2c and d. They interact with the OH groups of the (1 1 0) surface through a small number of low-coordination corner metal atoms. This also explains why bi-layer clusters (NBP or BBP) are not favorable: contrary to the (1 0 0) surface, they cannot maximize their number of M–O and M–Al bonds.

Fig. 3d and e displays the charge density difference isosurfaces for Pd_{13}–Pd_SA/(1 1 0) γ-Al_2O_3. As for dehydrated surfaces (Section 3.1.), all cluster atoms are electronically influenced by the support, although the metal atoms in direct contact with the hydroxyl groups are affected to the greatest extent.

The charge redistribution aims at minimizing the Pauli repulsion between occupied O 2p and Pd 4d orbitals. In Fig. 3d, Pd 4d and O 2p orbitals directed along the Pd–O bonds and responsible for direct overlap, become depopulated, while electrons are redistributed on other orbitals (Fig. 3e). Pd–O bonds are visible, as also shown by the ELF analysis (Fig. 3f) and the BOP values. Contrary to the dehydrated alumina surface, the BOP and ELF analysis do not reveal any covalent M–Al bonds. A previous study has shown that it is possible for a single Pd atom to directly interact with one Al atom of the (1 1 0) surface with the same surface density of hydroxyl groups [68]. In the present case, this interaction is prevented due to the M_{13} sterical bulkiness, which diminishes the accessibility of the Al atoms hidden by hydroxyls. Likewise, no evidence exists for any M–H bond with the hydrogen atoms of hydroxyl groups, which therefore interact only through their oxygen atoms.

Regarding the electrostatic charges, the Pd_{13} cluster becomes slightly cationic on the (1 1 0) surface, while the electron density on the aluminum atoms of the support is slightly increased. The Pt_{13} cluster is only very slightly anionic (this trend was more pronounced on (1 0 0)). There is thus a slight shift of the electrostatic charges of the clusters induced by the presence of the hydroxyl groups. For the sake of clarity, the distribution of charges in Pd_SA/(1 1 0) γ-Al_2O_3 and Pt_SA2/(1 1 0) γ-Al_2O_3 is reported and commented in Supplementary material S6.

The electrostatic charge analysis for the atoms of the support (Supplementary material S7) shows that, consistent with their participation in new M–O bonds, oxygen atoms directly bonded to M atoms are electronically depleted. Hence both partners in the bond are depleted, a clear demonstration of the Pauli repulsion release mechanism. Although not directly linked to metal atoms, aluminum atoms bearing the interacting OH groups are involved in the charge transfer: as for the dehydrated (1 0 0) surface, they become electronically enriched. Al atoms are indeed the sole electrophilic species, and play the role of indirect Lewis acid center, harvesting the electrons. This shows that although hydroxylation quenches the spreading of metal clusters on the support, it does not fully suppress the charge transfer between oxygen and aluminum atoms mediated by metal atoms.

Contrary to the dehydrated (1 0 0) alumina surface, the adsorption and interaction energies of Pd_{13} clusters are weaker than for smaller Pd_n (n = 1–5) clusters [69]. This also relates to longer Pd–O bonds and to the absence of any Pd–Al bonds for Pd_{13}, whereas they are possible for the smaller clusters. When the cluster's size increases, cluster trapping in OH pockets becomes impossible, so that the metal-support interaction is reduced to a surface interaction through only a few (3) Pd–O bonds. The small BOP values found for the M_{13}–(1 1 0) alumina interface confirm this interpretation (Supplementary material S2).

3.2.3. Migration of surface groups (OH, H) on the M_{13} clusters

Following some experimental [96] and theoretical [65,66,97,98] proposals of a possible reverse spillover of hydrogen coming from the surface hydroxyls and migration of hydroxyls to metal atoms, we have exhaustively investigated the transfer of H and OH of hydroxylated alumina (1 1 0) to the various sites (top, bridge, hollow) of Pd_SA and Pt_SA2. Note that our approach provides insights into the thermodynamic stability of the systems after eventual hydrogen reverse spillover, without considering kinetic limitations.

Any attempt to migrate the OH groups from the support to the M_{13} cluster failed to provide a more stable state than the reference one (deposited cluster as reported in the previous paragraph). This result shows that if such a process can be invoked for single Pt atoms [66], it is highly unfavorable for Pd_{13} and Pt_{13} clusters.

On the other hand, the migration of a single hydrogen atom from the support to the cluster leads to a thermodynamical stabilization of the system by −0.48 eV for the Pd_{13} adsorption energy and by −0.41 eV for Pt_{13} (corresponding to an increase in binding energies by about 0.03–0.04 eV/atom, see Table 1). For platinum, the migration of a second hydrogen atom is possible and leads to an additional stabilization of −0.28 eV (additional binding energy increase of 0.02 eV/atom). The protons from the intrinsically most acidic hydroxyls (associated with a weaker OH bond), e.g. μ_3-OH or μ_2-OH, are preferentially involved in this migration. On palladium, a hollow position (threefold coordinated) is preferred for the

hydrogen atom on the particle, whereas a top position is preferred for platinum. This compares well to the behavior of infinite (1 1 1) planes with respect to hydrogen reported in the literature (Pd(1 1 1) adsorbs H in a hollow position, whereas for Pt(1 1 1) hollow and top positions are competitive [99,100]). However, this phenomenon remains very limited since the migration becomes endothermic for the second and third hydrogen atoms to palladium and platinum, respectively. The most stable structures are depicted in Fig. 2c and d (lower part). Their energetic and geometric features are given in Table 1 (and Supplementary material S2). The migration of the proton slightly alters the shape of the metal Pd_{13} cluster, breaking one Pd–Pd bond, whereas the Pt_{13} cluster is almost unaffected. This migration gives rise to the formation of an additional weak M–O bond (confirmed by the ELF analysis, see Fig. 3g, and enhanced M–O BOP values), likely to be the cause of the stabilization. The fact that such a process is easier for Pt than for Pd is consistent with previous calculations undertaken for single atoms on α-Al_2O_3 [65,66], and for M_6 clusters in zeolites [98].

The electrostatic charge analysis (Table 1 and Supplementary material S6) shows that Pd and Pt clusters become cationic after spillover. The charge of the H atom is then close to zero, according to the Bader analysis, and slightly negative, according to Mulliken analysis, which contrasts with their cationic nature on the support. During the reverse spillover process, hydrogen thus acquires a hydride type nature, in agreement with previous results [98]. At the same time, the support is depleted of the positive charge corresponding to the missing proton. It can thus be deduced that a charge transfer occurs toward the hydrogen atoms (with a $H^{\cdot}$ or a $H^{\delta-}$ nature), concomitant with a charge depletion on the metallic cluster, in good relation with its formal oxidation.

4. Discussion

4.1. Models for highly dispersed Pt and Pd catalysts on γ-Al_2O_3: comparison with experiments

4.1.1. Preferred location of nanoparticles on the support

When obtained from the topotactic decomposition of boehmite AlO(OH), the predominant orientations of γ-Al_2O_3 nano-crystallites are (1 1 0) (about 70%) and (1 0 0) (about 20%) [21]. In usual operating conditions, the (1 0 0) surface of γ-Al_2O_3 is dehydrated, whereas the (1 1 0) surface remains partially hydrated [77,78]. Our results reveal that the expected geometry for M_{13} clusters closely depends on the hydration state of the exposed surfaces but also on the morphology of the γ-Al_2O_3 nano-crystallites (if the synthesis process allows it). Thus on the same support, several metallic particles shapes may co-exist on the surface, depending on the crystallographic orientation of the nano-crystallites and their hydroxylation states. This first insight inferred from our aforementioned results is crucial for experimentalists in order to describe more accurately the metallic cluster structure as a function of environment.

Our results first suggest that due to stronger metal-support interaction, Pd and Pt containing about 13 atoms are much more stabilized on the (1 0 0) surface of gamma-alumina than on the (1 1 0) one. Of course, as the full interaction of the metal precursors in aqueous solution has not been explicitly modeled here, we provide a picture of the stable nanoparticles, from a thermodynamic point of view after the calcination and reduction steps. This result is correlated to recent experimental observations on gamma-alumina [101]. On the anatase-TiO_2 support, surface orientation-dependant deposition of platinum particles has also been put in evidence [102]: in particular, the (1 0 1) surface of anatase-TiO_2 is the crystallographic plane where Pt particles are preferentially located. According to DFT calculations [103], the (1 0 1) anatase surface contains almost no hydroxyls after high temperature treatment: it is thus the one suspected to develop the stronger adsorption energy with metallic clusters, similarly as for the dehydrated gamma-alumina (1 0 0) surface. Such a selective dispersion of the metallic nanoparticles may be of high interest for electron–hole separation required in photocatalytic applications [102]. In bifunctional catalysis, it may also be of peculiar interest to optimize the location and distribution of the metallic function located on the (1 0 0) surface of γ-alumina in close connection with the Brønsted acid function provided by the hydroxyls of the (1 1 0) surface, by tuning the morphology of the γ-alumina particles.

4.1.2. Size effects

Concerning the impact of the size of the nanoparticles, although calculations reported in the present work have been performed at constant size, comparison with previous results for the palladium case [69] indicates that smaller Pd_n (n = 1–5) clusters are much more stabilized on (1 1 0) than on (1 0 0), due to the trapping of these small clusters into hydroxyl pockets of the (1 1 0) surface. This situation is not possible for larger (13 atoms) clusters. Even if further investigations are needed in particular to confirm if the trend can be transferred to platinum, smaller clusters M_n (n = 1–5) seem to be preferentially located on the hydrated (1 1 0) surface, whereas the larger particles (n = 13) would be more stabilized on the dehydrated (1 0 0). This result can be related to the observation of Freund et al. in the case of Rh clusters deposited on alumina film with various hydroxylation states [33].

It is, moreover, well known that ultra-dispersed palladium catalysts are much more difficult to obtain experimentally than their platinum analogs [48]. Our calculations show that the metal-support interaction is much stronger in the case of Pt than Pd, which may be an explanation of the experimental observation.

4.1.3. Structure of the catalysts and comparison with EXAFS data

For palladium, the contraction of the mean inter-atomic Pd–Pd distance to 2.713 Å (NBP/(1 0 0)) and 2.717 Å (Pd_SA/(1 1 0)) obtained in the present work is consistent with the 2.72 Å value experimentally obtained for the most dispersed samples reported in the literature [48]. The contraction of the lattice parameter when compared to the bulk is, however, always lower than for Pt catalysts [51] (see next paragraph), in agreement with our observations. This can be related to the larger loss of binding energy for platinum when lowering the M–M coordination, when compared to 12 in the bulk. Since Pt–Pt bond energy is stronger than Pd–Pd bond energy, stronger relaxation effects are thus expected for Pt clusters to compensate for the cohesion loss.

The Pd–Pd coordination numbers are 5.5 for NBP/(1 0 0) and 5.5–5.7 for Pd_SA/(1 1 0), (with and without reverse spillover respectively), and they compare well to the 4.9–5.9 range observed experimentally [48,51]. This is also true for all Pd_{13} structures reported in Table 1. Pd–O and mainly Pd–Al bonds are very scarcely reported in experimental data, as can be understood from our model which suggests that they are not numerous (N = 0.1) and mainly present on the dehydrated γ-Al_2O_3 (1 0 0) orientation accounting for 20% of the overall support surface.

For platinum clusters supported on alumina, a greater structural diversity is reported experimentally, depending on the preparation, reduction and pre-treatment conditions. Although the (1 0 0) alumina surface represents only 20% of the total support surface, a high affinity for platinum oxide has been demonstrated for the pentacoordinated aluminum atoms on γ-Al_2O_3 (1 0 0) [101], so that the models obtained for this orientation have to be considered. In the absence of hydrogen, inter-atomic Pt–Pt distances between 2.68 and 2.72 Å are often measured by EXAFS [41,42,44–46,49,104], in line with our calculated values: 2.69 Å for Pt_{13}-NBP/γ-Al_2O_3 (1 0 0) and 2.66 Å for Pt_SA2/γ-Al_2O_3 (1 1 0).

The latter value seems slightly too low when compared to experimental data. Meanwhile the inter-atomic Pt–Pt distances for the Pt_SA2/γ-Al_2O_3 (1 1 0) system increase slightly as reverse spillover of hydrogen occurs (Table 1), which suggests that traces of hydrogen in the environment (for example after *in situ* reduction followed by mild evacuation) will induce an expansion of the cluster. The GGA formalism generally overestimates metal–metal bond length in Pd and Pt clusters: the level of calculations cannot explain that most experimental values are slightly longer than calculated ones. Only an environment effect (remaining hydrogen) may explain that.

Experimentally, Pt–Pt coordination numbers vary significantly from 2 to 6.7 [41,42,44–46,49,104,105]. We indeed find a much broader range for the calculated *N* values reported in Table 1 (from 3.5 to 4.9) than in the case of palladium. Our supported Pt_{13} particle model thus appears as representative of most experimental studies in the field.

Two Pt–O bond distances are regularly reported by EXAFS [40–42,46,49,50,104]: the shorter one around 2.1–2.2 Å, matching nearly all our calculated structures, and a second one, significantly longer (from 2.5 to 2.7 Å) [40,41,50,104]. Up to now, it has been proposed to assign the latter to the presence of hydrogen between the support and the particles [41], inherent to residual hydrogen species after low temperature reduction but different from the hydrogen of hydroxyl groups, which is expected to increase the distance between oxygen atoms of the support and the particle. Indeed, as inferred by Vaarkamp et al. [41], we find very similar Pt–O bond lengths on the dehydrated and hydroxylated alumina surface, all smaller than 2.3 Å (corresponding to the first O-shell), whereas the second oxygen neighbor cannot match the experimental feature estimated at 2.7 Å (we calculate minimal Pt–O distances of 3.0 Å as second neighbors). It should be noted that the Pt–O distance in bulk PtO varies from 2.02 Å ($P_{4\_2/mmc}$, $N = 4$) [106] to 2.58 Å for the less common NaCl structure [107] ($F_{m\text{-}3m}$, $N = 6$). Moreover, the Pt–O coordination number reported experimentally for this component of the EXAFS data may vary with reported values of 0.5 [40], 1.2 [41] and up to 5.3 [50]. This is much higher than the values reported in Table 1, whereas it is six in the reference case of bulk PtO (NaCl structure). It can thus first be suspected that the largest EXAFS distance might originate from incomplete reduction of platinum or from a partial oxidation during the XAS experiment.

Vaarkamp et al. [41] invoke the possibility of alternative backscatters (other than oxygen), even though the possibility of aluminum atoms was eliminated due to the high temperatures required for the formation of PtAl alloys. However, our results suggest that the formation of platinum (palladium)–aluminum bonds of length 2.6–2.8 Å on the (1 0 0) alumina surface cannot be excluded, even without alloy formation. Such a new component could thus be introduced in future EXAFS analysis. We are aware that the average number of M–Al bonds is very low compared to the number of M–M bonds and also slightly lower than the number of M–O bonds. Therefore, it will not be an easy task to assess the contribution of Al atoms to the experimental EXAFS function in an XAS experiment. However, it can be proposed that the larger apparent Pt–O distance might result from the omission of Pt–Al features in the treatment of the EXAFS signal. At this stage, the assignment of this component to hydrogen between the support and the particles [41] or to water molecules on the particle itself [50] cannot be excluded. This will be the object of future studies (in particular modeling of hydrogen adsorption from the gas phase – different from reverse spillover – on the particles and at the particle/support interface).

4.1.4. Electronic charge of platinum catalyst particles

As concerns the charging of the metal cluster, information can be deduced from the white line intensities in XANES in principle (the higher the white line intensity, the higher the number of holes in the d band [108]). However, structure-induced charging is in fact most of the time convoluted with adsorbate effects, in particular due to residual hydrogen after reduction at variable temperature [41,42]. For the same reduction conditions and under He atmosphere, charge transfer from the support to the Pt particle has been observed [44,45], in agreement with the negative values of the charge reported for the Pt clusters, particularly on the (1 0 0) surface, in Table 1. The calculated cationic nature of the Pt cluster adsorbed on (1 1 0), especially after hydrogen reverse spillover, explains why experimental results are sometimes contradictory concerning this question. Moreover, the charge transfer from the metal to the hydrogen atom shown here could be of major importance when considering adsorbed H_2 on the clusters. Indeed, samples are usually obtained from reduction of oxide forms of the metals, so that hydrogen can *a priori* be adsorbed on the sample. As this may significantly affect the charging of the cluster, caution should be taken in interpreting the results. A detailed study of the behavior of the modeled particles under hydrogen will be the object of future work.

The present results thus give a representative picture of supported Pd and Pt catalysts, with small particle sizes, frequently encountered in the experimental literature. Our results suggest that M–Al, in particular Pt–Al bonds, should not be excluded in the interpretation of experimental data, in particular EXAFS. Moreover, reverse spillover of hydrogen from the hydroxyl groups to the metal particles may exist but only to a limited extent.

4.2. Particle shape models

Extrapolation of particle diameter from EXAFS data is often performed *via* a given particle shape model, with internal fcc packing [109]. This remains, however, a rather difficult task due to the high uncertainty on M–M coordination number. According to our present work, this is a reasonable assumption for the particles on dehydrated (1 0 0) alumina surfaces (Fig. 2a and b), even though a strong distortion, especially in the case of platinum, alters the real number of bonds when compared to a pure fcc phase. Moreover, some competitive structures (Supplementary material S3) are more closely related to the simple cubic than to fcc structure, which leads to lower coordination numbers (example: Pt_{13}-TCSC on (1 0 0)). Our models of M_{13} particles on the hydrated (1 1 0) surface also deviate from an ideal fcc closed-packed structure.

In particular, extrapolation of particle diameters from EXAFS data is often performed *via* a spherical shape model [40,50,109]. In the present work, we show that such an approach, although very approximate, is quite appropriate for hydrated (1 1 0) alumina surface (Fig. 2c and d), insofar as preferred particle morphologies are more or less three-dimensional (even if far from spherical), contrasting with the dehydrated (1 0 0) surface were clusters are almost flat (NBP structure, Fig. 2a and b). The disk model proposed by Greegor and Lytle is more appropriate in this case [109].

The flat shape (with height smaller than width) of clusters on dehydrated alumina surface is universally observed for model alumina supports (Pt or Pd clusters deposited on alumina films grown in the absence of water [23,24,26,28–30]). The smallest reported Pt clusters synthesized by these methods are typically 4 Å high and 10 Å wide [23,26], which compares quite well with the present 4.3 Å distance between the highest atom of the Pt_{13}-NBP/(1 0 0) γ-Al_2O_3 and the support, and with the 6.3 Å diameter of the particle. Indeed convolution of the tip shape in STM might increase the apparent diameter of the particles in the image.

From EXAFS analysis combined with geometrical models, Greegor and Lytle [109] reported for real Pt/Al_2O_3 catalysts a shape distribution (including sphere, cube or disk models) with a predominance of disks. This is in good agreement with the stable

shapes found in the present work and particularly with the higher stability of NBP-Pt_{13} on (1 0 0) γ-Al_2O_3.

Such DFT optimized models have some crucial consequences for the determination of the metal catalyst dispersion (defined as the ratio of surface atoms versus the total number of atoms in the particle). Whatever the model (sphere, cube, or disk), the dispersion should be close to unity for the very small particle sizes considered here [109]. This is true for the gas phase clusters, all atoms being on the outer shell, but some atoms become inaccessible upon deposition on the support. For example on M_{13}/(1 0 0) γ-Al_2O_3 (Fig. 2a and b), the lowermost central atom is *a priori* not accessible to external molecules. In addition, the models found in our study highlight the importance of not only quantifying the number of exposed metallic atoms but also identifying the metallic atoms interacting with the support. On the (1 0 0) surface, 7/13 atoms are directly bound with the support, compared to only 3/13 on the (1 1 0) surface. In both cases, this changes drastically the accessibility of the metal sites and the electronic properties of the clusters.

4.3. Origin of the metal support interaction

The present work provides insight into the nature of the metal-support interaction for γ-Al_2O_3-supported Pd and Pt catalysts. We show the presence of a variable number of M–O and M–Al bonds between the cluster and the oxide. Fig. 4 illustrates that the corresponding BOP (summed over all bonds between the cluster and the oxide) is well correlated to the interaction energy of the cluster on the support. This shows that the interaction between the two species is driven by the formation of these bonds. The adsorption energy shows little correlation with the total BOP value, especially for the highly distorted clusters (when compared to the gas phase). The preferred morphology of a supported cluster in this size range ($\sim$13 atoms) is determined by its ability to maximize the number of strong M–O and possibly M–Al bonds with the alumina support. Depending on the density and spatial arrangement of the "host" O and Al atoms, the morphology will be preferentially flat (high density of binding atoms on the support on the flat (1 0 0) alumina surface) or three-dimensional (interacting by a few corners on the hydrated (1 1 0) alumina surface where only the most external OH groups can interact with the cluster).

The trend in the morphological changes of the small M_{13} clusters can also be regarded in light of the wetting parameter of the support by the metallic particles [110]. This parameter is directly linked to the metal-support interaction energy, and it helps to quantify the geometrical contact angle between a metallic particle and the support: the stronger the wetting, the smaller the contact angle. Our recent study [69] has shown that for gamma-alumina, the wetting parameter of palladium depends on the hydroxylation state of the γ-alumina surface. In particular, the adhesion energy of a palladium film was significantly weaker for hydroxylated surfaces than for the non-hydroxylated one. This trend is consistent with the morphologies found in the present study. On the non-hydroxylated (1 0 0) surface, leading to stronger intrinsic adhesion of a metallic film, the wetting of the surface by M_{13} clusters is expected to be high and thus flat bi-planar morphologies (NBP) are expected to be predominant, leading to high contact area or low "contact angle" (in as much as it can be defined for such small systems). In contrast, on the (1 1 0) surface the wetting is intrinsically weakened by the presence of hydroxyls. As a consequence, the metallic particles with a three-dimensional like morphology (low contact area and higher contact angle) preferentially remain on top of the hydroxyl layers.

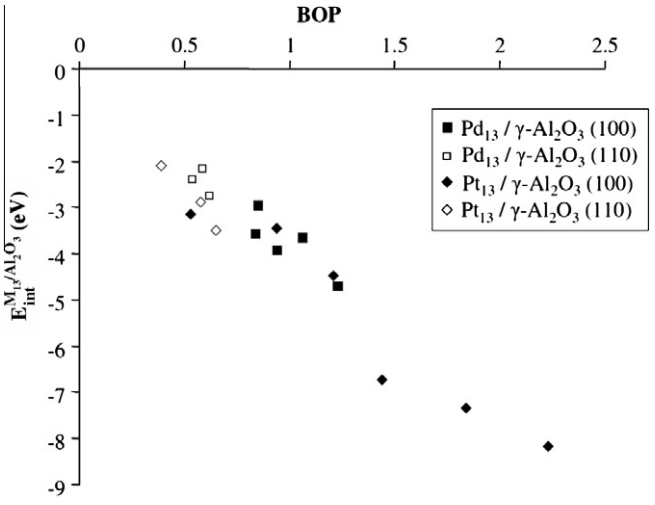

Fig. 4. Interaction energy $E_{int}^{M_{13}/Al_2O_3}$ of the stable clusters on alumina (1 0 0) (dehydrated) and (1 1 0) (hydrated) surfaces, as a function of the BOP value (summed over all M–O and M–Al bonds at the M_{13}/Al_2O_3 interface).

4.4. Insights into the reactivity of highly dispersed Pd and Pt catalysts

Due to the combined effects of size and support, 13-atoms clusters supported on γ-Al_2O_3 surfaces exhibit features very different from those of larger particles, which may have major impact in catalysis. First, a great variety of morphologies is revealed by the gas phase study [76], including very low coordination of metal atoms, below 6 on average (3 in Pt_SA2 for example). It can be expected that the adsorption and activation of reactive molecules will be strongly affected by such typical local environment of metallic sites, with respect to ideal metallic (1 1 1) or (1 0 0) surface sites (with coordination number of 8–9) or to stepped surfaces (M–M coordination number close to 7).

Support effects, in the present case induced by gamma-alumina, consist in structural and electronic effects, which are shown to be closely interconnected, even if their contribution may depend on the oxide surface on which the clusters are deposited. On the dehydrated (1 0 0) surface of gamma-alumina, the preferred clusters exhibit bi-planar geometry, with mainly triangular facets similar to (1 1 1) compact planes of large particles. At the same time, seven metal atoms at the metal-support interface are in strong interaction with the support, which may significantly perturb their reactivity (from an electronic and sterical point of view). In contrast, the six upmost metal atoms remain freely available for reactant molecules. In addition, from the electrostatic charge analysis, an overall increase in the nucleophilicity of the metal atoms is expected. On the hydrated γ-Al_2O_3 (1 1 0) surface, as 3D clusters exhibiting prominent corners are stabilized, coordination effects are expected to be even stronger than on the dehydrated surface. In that case, only 3–4 metal atoms are expected to develop strong metal-support interactions at the interface. These metal atoms interacting with hydroxyls become clearly positively charged, whereas the other metal atoms located further from the interface are more nucleophilic centers. These nucleophilic centers, are however, converted into electrophilic centers after hydrogen atoms are transferred from surface hydroxyls, following a reverse spillover process. In that case, the M_{13} clusters become cationic.

As a consequence, the electronic and structural properties of the original metallic sites of M_{13} clusters are intimately sensitive to the nature and state of the support's surface.

5. Conclusions

This work has proposed a DFT study of the thermodynamic stability of relevant M_{13} clusters (M = Pd and Pt) deposited on fully

dehydrated (1 0 0) and partially hydroxylated (1 1 0) γ-alumina surfaces which are known to exist in catalytic reaction conditions. On the non-hydroxylated (1 0 0) surfaces, we have shown that the bi-planar Pd and Pt clusters are favored to the detriment of other clusters with a three-dimensional morphology. For Pt_{13}, the preferred shape on this surface is hence modified when compared to the gas phase. In contrast, on the (1 1 0) surface, the reverse trend is observed, due to the presence of hydroxyl groups which weakens the interaction energy of the metallic cluster with the surface. On this hydroxylated surface, reverse spillover of the protons to the metal cluster is shown to occur but to a limited extent (at most two hydrogen atoms for 13 metal atoms). Moreover, a detailed electronic analysis (based on charge density differences, Electron Localization Function and Bond Overlap Population calculations) has enabled a rationalization of the energetic trend on the basis of the different chemical bonds formed at the interface between the clusters and the surface. We have also highlighted how the newly proposed models may help in the interpretation of X-ray absorption spectroscopy data. Our results demonstrate that several structures may co-exist depending on the surface orientation for instance. In addition, some structures are very close in energy which suggests that they could co-exist at ambient temperature. Since EXAFS structural determination is a global analysis and very sensitive to the structural inhomogeneity of the samples, our theoretical results could be used to facilitate the experimental analysis. In particular, we show that the formation of M–O bonds together with M–Al bonds should be taken into account as they exist on the (1 0 0) surface.

The nature of the interface also has an impact on the charge of the cluster metal atoms. In particular, on the (1 0 0) surface, Pt clusters may become negatively charged, while Pd clusters remain globally neutral but strongly polarized. In contrast, on the hydroxylated (1 1 0) surface, the clusters become positively charged. The hydroxylated surface hence shows an enhanced electro-attractive character. Furthermore, a clear correlation has been established between the interaction energies and the BOP electronic parameters calculated for the bonds located at the interface, confirming that the strength of the interaction depends on the new chemical bonds formed at the interface and hence that the adhesion is mainly of covalent nature. This electronic behavior is crucial for a better understanding of the catalytic reactivity which is suspected to depend on the following parameters:

- the presence of hydroxyls, which change the electronic properties of the metallic clusters,
- the position of the active metallic site on the particles, which confers either a cationic or an anionic behavior, depending on its position with respect to the support interface.

In a more general perspective, our study thus highlights the stabilization of highly undercoordinated metal sites present on metallic clusters dispersed on a relevant support, such as γ-alumina. These highly uncoordinated metal sites, not present on large metallic particles exposing terraces or even steps, are expected to be at the center of peculiar activation processes. These models constitute a solid basis for further theoretical investigation of the reactivity under hydrogen pressure. It is suspected that these environmental conditions will impact the morphology and electronic properties of such small clusters.

Acknowledgments

All calculations have been performed at IFP, CINECA, and IDRIS/CINES HPC centers within the Project x2010086134 funded by GENCI. This work has also been performed within the SIRE Project (ANR-06-CIS6-014-04) funded by the Agence Nationale de la Recherche (ANR).

The authors would like to thank their IFP colleague, Dr. J. Lynch, who passed away abruptely on May 28th, 2010, for his usual willingness and deep scientific competence. John often acted as an helpful internal reviewer including for the present report.

Appendix A. Supplementary material

Supplementary data associated with this article can be found, in the online version, at doi:10.1016/j.jcat.2010.06.009.

References

[1] B.C. Gates, Chem. Rev. 95 (1995) 511.
[2] J.H. Sinfelt, Catalytic reforming, in: G. Ertl, E. Knözinger, J. Weitkamp (Eds.), Handbook of Heterogeneous Catalysis, Wiley, Weinheim, 1997, p. 1939.
[3] A.T. Bell, Science 299 (2003) 1688.
[4] H.-J. Freund, Surf. Sci. 500 (2002) 271.
[5] C.T. Campbell, J. Chem. Soc., Faraday Trans. 92 (1996) 1435.
[6] Z. Xu, F.S. Xiao, S.K. Purnell, O. Alexeev, S. Kawi, S.E. Deutsch, B.C. Gates, Nature 372 (1994) 346.
[7] M. Haruta, Catal. Today 36 (1997) 153.
[8] M.K. Oudenhuijzen, J.A. van Bokhoven, J.T. Miller, D.E. Ramaker, D.C. Koningsberger, J. Am. Chem. Soc. 127 (2005) 1530.
[9] D. Matthey, J.G. Wang, S. Wendt, J. Matthiesen, R. Schaub, E. Laegsgaard, B. Hammer, F. Besenbacher, Science 315 (2007) 1692.
[10] K. Shimizu, R. Sato, A. Satsuma, Angew. Chem. Int. Ed. 48 (2009) 3982.
[11] C.R. Henry, Surf. Sci. Rep. 31 (1998) 231.
[12] J. Lynch, Oil Gas Sci. Technol. – Rev. IFP 57 (2002) 281.
[13] A.K. Santra, D.W. Goodman, J. Phys.: Condens. Matter 14 (2002) R31.
[14] P.D. Nellist, S.J. Pennycook, Science 274 (1996) 413.
[15] A.I. Frenkel, C.W. Hills, R.G. Nuzzo, J. Phys. Chem. B 105 (2001) 12689.
[16] A.M.J. van der Eerden, T. VIsser, A. Nijhuis, Y. Ikeda, M. Lepage, D.C. Koningsberger, B.M. Weckhuysen, J. Am. Chem. Soc. 127 (2005) 3272.
[17] M. Sterrer, T. Risse, L. Giordano, M. Heyde, N. Nuilius, H.P. Rust, G. Pacchioni, H.-J. Freund, Angew. Chem. Int. Ed. 46 (2007) 8703.
[18] R.E. Winans, S. Vajda, G.E. Ballentine, J.M. Elam, B. Lee, M.J. Pellin, S. Seifert, G.Y. Tikhonov, N.A. Tomczyk, Topics Catal. 39 (2006) 145.
[19] S. Vajda, M.J. Pellin, J.P. Greeley, C.L. Marshall, L.A. Curtiss, G.E. Ballentine, J.M. Elam, S. Catillon-Mucherie, P.C. Redfern, F. Mehmood, P. Zapol, Nat. Mater. 8 (2009) 213.
[20] H. Häkkinen, S. Abbet, A. Sanchez, U. Heiz, U. Landman, Angew. Chem. Int. Ed. 42 (2003) 1297.
[21] P. Euzen, P. Raybaud, X. Krokidis, H. Toulhoat, J.L. Loarer, J.-P. Jolivet, C. Froidefond, Alumina, in: F. Schüth, K.S.W. Sing, J. Weitkamp (Eds.), Handbook of Porous Solids, Wiley-VCH, Weinheim, 2002.
[22] F. Winkelmann, S. Wohlrab, J. Libuda, M. Bäumer, D. Cappus, M. Menges, K. Al-Shamery, H. Kuhlenbeck, H.-J. Freund, Surf. Sci. 307–309 (1994) 1148.
[23] T. Bertrams, F. Winkelmann, T. Uttich, H.-J. Freund, H. Neddermeyer, Surf. Sci. 331–333 (1995) 1515.
[24] M. Klimenkov, S.A. Nepijko, H. Kuhlenbeck, M. Bäumer, R. Schlögl, H.-J. Freund, Surf. Sci. 391 (1997) 27.
[25] K.H. Højrup Hansen, T. Worren, S. Stempel, E. Laegsgaard, M. Baeumer, H.J. Freund, F. Besenbacher, I. Stensgaard, Phys. Rev. Lett. 83 (1999) 4120.
[26] M. Klimenkov, H. Kuhlenbeck, S.A. Nepijko, Surf. Sci. 539 (2003) 31.
[27] N. Nilius, T.M. Wallis, W. Ho, Phys. Rev. Lett. 90 (2003) 046808.
[28] S.D. Sartale, H.W. Shiu, M.H. Ten, J.Y. Huang, M.F. Luo, Surf. Sci. 600 (2006) 4978.
[29] M.F. Luo, W.H. Wen, C.S. Lin, C.I. Chiang, S.D. Sartale, M.S. Zei, Surf. Sci. 601 (2007) 2139.
[30] E. Napetschnig, M. Schmid, P. Varga, Surf. Sci. 601 (2007) 3233.
[31] A. Stierle, F. Renner, R. Streitel, H. Dosch, W. Drube, B.C. Cowie, Science 303 (2004) 1652.
[32] G. Kresse, M. Schmid, E. Napetschnig, M. Shishkin, L. Köhler, P. Varga, Science 308 (2005) 1440.
[33] M. Heemeier, M. Frank, J. Libuda, K. Wolter, H. Kuhlenbeck, M. Bäumer, H.J. Freund, Catal. Lett. 68 (2000) 19.
[34] L. Giordano, G. Pacchioni, Surf. Sci. 575 (2005) 197.
[35] M. Sterrer, M. Yulikov, E. Fischbach, M. Heyde, H.P. Rust, G. Pacchioni, T. Risse, H.-J. Freund, Angew. Chem. Int. Ed. 45 (2006) 2630.
[36] X.G. Gong, A. Selloni, O. Dulub, P. Jacobson, U. Diebold, J. Am. Chem. Soc. 130 (2008) 370.
[37] B.N. Shelimov, J.F. Lambert, M. Che, B. Didillon, J. Mol. Catal. A 158 (2000) 91.
[38] J.H. Sinfelt, G.H. Via, F.W. Lytle, J. Chem. Phys. 68 (1978) 2009.
[39] G.H. Via, J.H. Sinfelt, F.W. Lytle, J. Chem. Phys. 71 (1970) 690.
[40] A. Munoz-Paez, D.C. Koningsberger, J. Phys. Chem. 99 (1995) 4193.
[41] M. Vaarkamp, J.T. Miller, F.S. Modica, D.C. Koningsberger, J. Catal. 163 (1996) 294.
[42] M.K. Oudenhuijzen, J.H. Bitter, D.C. Koningsberger, J. Phys. Chem. B 105 (2001) 4616.
[43] E. Bus, J.A. van Bokhoven, Phys. Chem. Chem. Phys. 9 (2007) 2894.

[44] J.H. Kang, L.D. Menard, R.G. Nuzzo, A.I. Frenkel, J. Am. Chem. Soc. 128 (2006) 12068.
[45] S.I. Sanchez, L.D. Menard, A. Bram, J.H. Kang, M.W. Small, R.G. Nuzzo, A.I. Frenkel, J. Am. Chem. Soc. 131 (2009) 7040.
[46] A. Bensaddik, A. Caballero, D. Bazin, H. Dexpert, B. Didillon, J. Lynch, Appl. Catal. A 162 (1997) 171.
[47] M. Womes, T. Cholley, F. Le Peltier, S. Morin, B. Didillon, N. Szydlowski-Schildknecht, Appl. Catal. A 283 (2005) 9.
[48] M. Benkhaled, S. Morin, C. Pichon, C. Thomazeau, C. Verdon, D. Uzio, Appl. Catal. A 312 (2006) 1.
[49] O.S. Alexeev, F. Li, M.D. Amiridis, B.C. Gates, J. Phys. Chem. B 109 (2005) 2338.
[50] A. Siani, K.R. Wigal, O.S. Alexeev, M.D. Amiridis, J. Catal. 257 (2008) 16.
[51] M.W. Tew, J.T. Miller, J.A. van Bokhoven, J. Phys. Chem. C 113 (2009) 15140.
[52] C. Verdozzi, D.R. Jennison, P.A. Schultz, M.P. Sears, Phys. Rev. Lett. 82 (1999) 799.
[53] Z. Lodziana, J.K. Nørskov, J. Chem. Phys. 115 (2001) 11261.
[54] Z. Lodziana, J.K. Nørskov, Surf. Sci. 518 (2002) L577.
[55] J.R.B. Gomes, F. Illas, N. Cruz Hernandez, F.J. Sanz, A. Wander, N.M. Harrison, J. Chem. Phys. 116 (2002) 1684.
[56] J.R.B. Gomes, F. Illas, N. Cruz Hernandez, A. Marquez, F.J. Sanz, Phys. Rev. B 65 (2002) 125414.
[57] J.R.B. Gomes, Z. Lodziana, F. Illas, J. Phys. Chem. B 107 (2003) 6411.
[58] J.R.B. Gomes, F. Illas, B. Silvi, Chem. Phys. Lett. 388 (2004) 132.
[59] V.V. Rivanenkov, V.A. Nasluzov, A.M. Shor, K.M. Neyman, N. Rösch, Surf. Sci. 525 (2003) 173.
[60] V.A. Nasluzov, V.V. Rivanenkov, A.M. Shor, K.M. Neyman, N. Rösch, Chem. Phys. Lett. 374 (2003) 487.
[61] D.R. Jennison, T.R. Mattsson, Surf. Sci. 544 (2003) L689.
[62] B. Hinnemann, E.A. Carter, J. Phys. Chem. C 111 (2007) 7105.
[63] C. Zhou, J. Wu, T.J.D. Kumar, N. Balakrishnan, R.C. Forrey, H. Cheng, J. Phys. Chem. C 111 (2007) 13786.
[64] L.G.V. Briquet, C.R.A. Catlow, S.A. French, J. Phys. Chem. C 112 (2008) 18948.
[65] L.G.V. Briquet, C.R.A. Catlow, S.A. French, J. Phys. Chem. C 113 (2009) 16747.
[66] L. Xiao, W.F. Schneider, Surf. Sci. 602 (2008) 3445.
[67] X. Krokidis, P. Raybaud, A.E. Gobichon, B. Rebours, P. Euzen, H. Toulhoat, J. Phys. Chem. B 105 (2001) 5121.
[68] M. Corral Valero, P. Raybaud, P. Sautet, J. Phys. Chem. B 110 (2006) 1759.
[69] M. Corral Valero, P. Raybaud, P. Sautet, Phys. Rev. B 75 (2007) 045427.
[70] N.A. Deskins, D. Mei, M. Dupuis, Surf. Sci. 603 (2009) 2793.
[71] A.M. Marquez, F.J. Sanz, Appl. Surf. Sci. 238 (2004) 82.
[72] R. Ishimoto, C. Jung, H. Tsuboi, M. Koyama, A. Endou, M. Kubo, C.A. Del Carpio, A. Miyamoto, Appl. Catal. A 305 (2006) 64.
[73] F. Vila, J.J. Rehr, J. Kas, R.G. Nuzzo, A.I. Frenkel, Phys. Rev. B 78 (2008) 121404.
[74] F. Ahmed, M.K. Alam, A. Suzuki, M. Koyama, H. Tsuboi, N. Hatakeyama, A. Endou, H. Takaba, C.A. Del Carpio, M. Kubo, A. Miyamoto, J. Phys. Chem. C 113 (2009) 15676.
[75] M. Corral Valero, P. Raybaud, P. Sautet, J. Catal. 247 (2007) 339.
[76] C.H. Hu, C. Chizallet, H. Toulhoat, P. Raybaud, Phys. Rev. B 79 (2009) 195416.
[77] M. Digne, P. Sautet, P. Raybaud, P. Euzen, H. Toulhoat, J. Catal. 211 (2002) 1.
[78] M. Digne, P. Sautet, P. Raybaud, P. Euzen, H. Toulhoat, J. Catal. 226 (2004) 54.
[79] J. Joubert, P. Fleurat-Lessard, F. Delbecq, P. Sautet, J. Phys. Chem. B 110 (2006) 7392.
[80] J. Hietala, A. Root, P. Knuuttila, J. Catal. 150 (1994) 46.
[81] G. Kresse, J. Hafner, Phys. Rev. B 49 (1994) 14251.
[82] G. Kresse, J. Furthmüller, Phys. Rev. B 54 (1996) 11169.
[83] J. Perdew, Y. Wang, Phys. Rev. B 45 (1992) 13244.
[84] P.E. Blöchl, Phys. Rev. B 50 (1994) 17953.
[85] G. Kresse, D. Joubert, Phys. Rev. B 59 (1999) 1758.
[86] S.H. Vosko, L. Wilk, M. Nusair, Can. J. Phys. 58 (1980) 1200.
[87] A. Savin, A.D. Becke, J. Flad, R. Nesper, H. Preuss, H.G. von Schnering, Angew. Chem. Int. Ed. 30 (1991) 409.
[88] B. Silvi, A. Savin, Nature 371 (1994) 683.
[89] G. Henkelman, A. Arnaldsson, H. Jonsson, Comput. Mater. Sci. 36 (2006) 354.
[90] E. Sanville, S.D. Kenny, R. Smith, G. Henkelman, J. Comput. Chem. 28 (2007) 899.
[91] M.D. Segall, R. Shah, C.J. Pickard, M.C. Payne, Phys. Rev. B 54 (1996) 16317.
[92] S.J. Clark, M.D. Segall, C.J. Pickard, P.J. Hasnip, M.I.J. Probert, K. Refson, M.C. Payne, Z. Kristallogr. 220 (2005) 567.
[93] J.R. Yates, C.J. Pickard, F. Mauri, Phys. Rev. B 76 (2007) 024401.
[94] D. Sanchez-Portal, E. Artacho, J.M. Soler, Solid State Commun. 95 (1995) 685.
[95] R.S. Mulliken, J. Chem. Phys. 23 (1955) 1833.
[96] W.C.J. Conner, J.L. Falconer, Chem. Rev. 95 (1995) 759.
[97] G.N. Vayssilov, B.C. Gates, N. Rösch, Angew. Chem. Int. Ed. 42 (2003) 1391.
[98] G.N. Vayssilov, N. Rösch, Phys. Chem. Chem. Phys. 7 (2005) 4019.
[99] R.A. Olsen, G.J. Kroes, E.J. Baerends, J. Chem. Phys. 111 (1999) 11155.
[100] G.W. Watson, R.P.K. Wells, D.J. Willock, G.J. Hutchings, J. Phys. Chem. B 105 (2001) 4889.
[101] J.H. Kwak, J. Hu, D. Mei, C.W. Yi, D.H. Kim, C.H.F. Peden, L.F. Allard, J. Szanyi, Science 325 (2009) 1670.
[102] T. Ohno, K. Sarukawa, M. Matsumura, New J. Chem. 26 (2002) 1167.
[103] C. Arrouvel, M. Digne, M. Breysse, H. Toulhoat, P. Raybaud, J. Catal. 222 (2004) 152.
[104] J.R. Chang, S.L. Chang, T.B. Lin, J. Catal. 169 (1997) 338.
[105] B.J. Kip, F.B.M. Duivenvoorden, D.C. Koningsberger, R. Prins, J. Catal. 105 (1987) 26.
[106] W.J. Moore, L. Pauling, J. Am. Chem. Soc. 63 (1941) 1392.
[107] J. Kumar, R. Saxena, J. Less Common Metals 147 (1989) 59.
[108] J.H. Sinfelt, G.D. Meitzner, Acc. Chem. Res. 26 (1993) 1.
[109] R.B. Greegor, F.W. Lytle, J. Catal. 63 (1980) 476.
[110] C.R. Henry, Prog. Surf. Sci. 80 (2005) 92.